Astron. Astrophys. 355, 333–346 (2000)

ASTRONOMY AND ASTROPHYSICS

The structure and stability of interstellar molecular absorption line profiles at radio frequencies

H. Liszt[1] **and R. Lucas**[2]

[1] National Radio Astronomy Observatory, 520 Edgemont Road, Charlottesville, VA 22903-2475, USA
[2] Institut de Radioastronomie Millimétrique, 300 Rue de la Piscine, 38406 Saint Martin d'Hères, France

Received 29 September 1997/Accepted 11 January 2000

Abstract. We have taken new, broader-band and higher-resolution profiles of Galactic 1667 MHz OH and 89.2 GHz HCO^+ absorption toward several compact, extragalactic mm-wave continuum sources. The profiles are generally stable – quite similar between epochs and between the two species – but with occasional time-variations and differences. Typical linewidths are 1.0 km s^{-1} (FWHM) in either OH or HCO^+ and there are no differences in mean velocity. Profiles are compound but do not show broad wings, multiplicity, assymmetry, or other phenomena strikingly indicative of formation under extraordinary circumstances, consistent with the low ambient thermal pressures reflected in the weak rotational excitation of CO and HCO^+.

However, we have also discovered the existence of a low-lying, broad component of HCO^+ absorption covering just those portions of the spectrum where $\tau_{\rm HI} \geq 0.1 - 0.2$ at $\lambda 21$ cm. Toward B0355+508 at $b = -1.6$ °, HCO^+ absorption extends continuously over more than 40 km s^{-1}. The broadly-distributed HCO^+ absorption can be understood in terms of the known molecular fraction of local gas, as long as HCO^+ is generally present at about its typical abundance n(HCO^+)/n(H_2) = 2×10^{-9}. The fact that CO forms rapidly from HCO^+ in diffuse gas then suffices to account for the abundance of CO in diffuse/translucent material over the entire range $10^{12} \leq N({\rm CO}) \leq 10^{16}$ cm^{-2}, $10^{19} \leq {\rm H_2} \leq 10^{21}$ cm^{-2}, using otherwise standard cloud models.

Using models of molecular formation and excitation and the H-H_2, C^+-CO transition in diffuse gas, and noting the absence of HCO^+ emission at levels of 0.02-0.05 K, we show very directly that the line profile variations are not the result of AU-sized inclusions of high hydrogen volume density, in the manner usually inferred. Instead, it is necessary to account for small-scale chemical and other inhomogeneities.

Key words: ISM: abundances – ISM: molecules – ISM: structure – radio lines: ISM

Send offprint requests to: H. Liszt
Correspondence to: hliszt@nrao.edu

1. Introduction

Following the discovery of Galactic λ2.6mm CO absorption toward BL Lac (B2200+420) by Marscher et al. (1991), we subsequently found that a wide variety of molecules could be studied in absorption in the nearby diffuse/translucent gas seen toward extragalactic compact mm-wave continuum sources (Lucas and Liszt 1993, 1994). Indeed, a survey of HCO^+ absorption (Lucas and Liszt 1996) found that it is much more frequent than CO emission, and remarkably common, even compared to HI, at Galactic latitudes below $15^{\rm o}-20^{\rm o}$. The abundances of polyatomics like C_3H_2 (Cox et al. 1988), HCO^+, HCN, C_2H are much higher than can be explained by even the most exhaustive conventional chemical models (Van Dishoeck and Black 1988) unless the gas is taken to be denser (Viala et al. 1988) than we believe to be the case (Liszt and Lucas 1998).

The need to promote more rapid chemical formation in diffuse gas threaded by a strong UV radiation field has given rise to consideration of shock models (Flower and Pineau Des Forêts 1998) and somewhat more exotic schemes involving local dissipation of turbulent energy (Joulain et al. 1998). The shock models in particular imprint distinct kinematic signatures on resultant line profiles, and the existence of any kinematic peculiarities can of course be tested very directly given the high spectroscopic resolving power of modern instruments.

In an attempt to understand better the nature of the absorption profiles we have been studying, and especially to see if in these spectra there are signs of the underlying molecular formation mechanisms, we have taken spectra of OH and HCO^+ which have some combination of higher-resolution, broader-bandwidth, and higher sensitivity. These spectra can be compared with each other and with their predecessors, to study their structure and stability (similarity across time and species). It seems to be the case that absorption profiles from the interstellar neutral gas vary on yearly time scales and on AU-sized spatial scales across a wide range of experiments, for instance, in atomic hydrogen absorption mapped on VLB scales (Diamond et al. 1989; Faison et al. 1998) or in H_2CO absorption measured toward point-sources at various epochs (Moore and Marscher 1995). The physical conditions inferred

from a naive analysis of these variations, with densities hypothesized to range up to 10^6 cm^{-3}, should surely have some discernible consequences.

Sect. 2 describes the observational material used here. Sect. 3 compares HCO^+ and OH profiles across time and species. Sect. 4 presents equilibrium models of the H-H_2 and C^+-CO transitions in diffuse gas. Using these models, it discusses the distributed, Galactic scale contribution to molecular absorption profiles, and shows that the observed abundances of CO are the natural result of a high abundance of HCO^+ in weakly molecular gas. Sect. 5 questions the viability of dense inclusions in neutral gas clouds, which have often been inferred from the yearly time scales or milli-arcsecond spatial scales on which absorption profiles (like ours) appear to vary. The weakness of HCO^+ emission is a very strong constraint on the internal structure of diffuse clouds.

2. Observations

2.1. VLA observations of 1667MHz OH

Earlier we took OH spectra at the VLA but with an inadvertantly mis-set bandwidth code, which permitted only a measurement of the integrated absorption in the resultant spectra (Liszt and Lucas 1996). This dataset, and a subsequent OH spectrum acquired at Nançay (the latter normalized to VLA data provided by A. Marscher) enabled the discovery of a tight, linear OH-HCO^+ correlation but provided little kinematic information otherwise. This situation was rectified in 1998 August when we used the VLA to observe 1667.359 MHz OH absorption toward the sources listed in Table 1 with the narrowest possible resolution 763Hz, or 0.137 km s^{-1}. To do so required not using on-line smoothing.

We observed bandpass calibrators (3C286, 3C48) every few hours and spent 1-4 hours on each source. No phase calibrators were observed and the data are entirely self-calibrated. As in our earlier work, an AIPS task UVLSD formed the final spectra as line/continuum ratios, by continuous weighted averaging of the data, without recourse to external phase calibration. All the sources studied here are point-source VLA calibrators, except for 3C111 which has weak extended structure. Moore and Marscher (1995) show profiles at various positions over this source.

Toward B0212+735, the bluer half of the bandpass could not be used, owing to some instability which induced a strong curvature. Toward B0355+508, the signal/noise turned out somewhat lower than we hoped (although still better than our previous spectrum from Nançay) and perhaps with some low-level fluctuations in the baseline. The sources toward which we have acquired new OH observations are listed in Table 1 along with the rms noise in line/continuum at the spectral baseline. Profile integrals are given in Table 2 for the new and old data.

2.2. Plateau de Bure Interferometer observations of HCO^+

Compared to six years ago when we began this work, the Plateau de Bure Interferometer has five rather than three antennas, better receivers, and higher spectral resolution. We took new HCO^+ spectra of the sources listed in Table 1 using correlators configured for 140 kHz resolution sampled at 78.1 kHz (0.47 and 0.26 km s^{-1}, respectively) and 70 kHz resolution sampled at 39.1 kHz. As earlier, the baseline established for a broader band was interpolated to and subtracted from the line-bearing regions of the spectrum. In many cases, the HCO^+ absorption extended beyond the range of the higher-resolution data. The broad underlying HCO^+ absorption toward B0355+508 and B0415+379 was, in retrospect, present in our earlier data. The sources for which we have new HCO^+ profiles are listed in Table 1. The rms error in the baseline line/continuum ratio pertains to the higher-resolution data. Profile and optical depth integrals for the new and old data are given in Table 3.

Table 1. Background Sources and Line/Continuum Rms

Source	Alias	l ^{o}	b ^{o}	$\sigma_{l/c}$ OH	$\sigma_{l/c}$ HCO^+
B0212+735		128.93	11.96	0.0034	
B0355+508	N150	150.38	−1.60	0.0040	0.0073
B0415+379	3C111	161.68	−8.82	0.0090	0.0105
B0528+134		191.37	−11.01		0.0100
B1730−130	N530	12.03	10.81	0.0015	0.0119
B1954+513		85.30	121.76	0.0044	0.0281
B2200+420		92.13	−10.40	0.0030	0.0156

2.3. Extant observations of atomic hydrogen emission and absorption, and CO absorption in the UV

The HI emission profiles displayed here are from the Leiden-Dwingeloo all sky survey of (Hartmann and Burton 1997). The absorption profiles are those of (Dickey et al. 1983) and (Garwood and Dickey 1989), courtesy of J. Dickey and B. Garwood. CO column densities measured in UV absorption are from an updated version (from Federman) of the summary in (Federman et al. 1994).

3. OH and HCO^+ profiles, then and now

3.1. Stability of HCO^+ absorption over 3–5 year intervals

New and old profiles of HCO^+ absorption in the 78 kHz channel spectra are shown and differenced in Figs. 1 and 2. Profiles of the line optical depth and optical depth differences are shown for three sources in Fig. 3.

In several cases, small imperfections in the spectral baseline are manifested across the difference specta. For components as broad as some of those seen here this could be easily misconstrued. But the red wings of the -17 km s^{-1} and -4 km s^{-1} components toward B0355+508, the entire stronger line toward B0528+134, and the central region of the deep line toward B2200+420 have statistically significant differences. The -4 km s^{-1} component toward B0355+508 noticeably changes its shape. All the variation toward this source represent changes in the profile integrals. Toward B0528+134 and B2200+420 the variations have the characteristic, partially integral-conserving up-down shape of a simple shift in velocity (though we cannot be certain that this is in fact what has occurred).

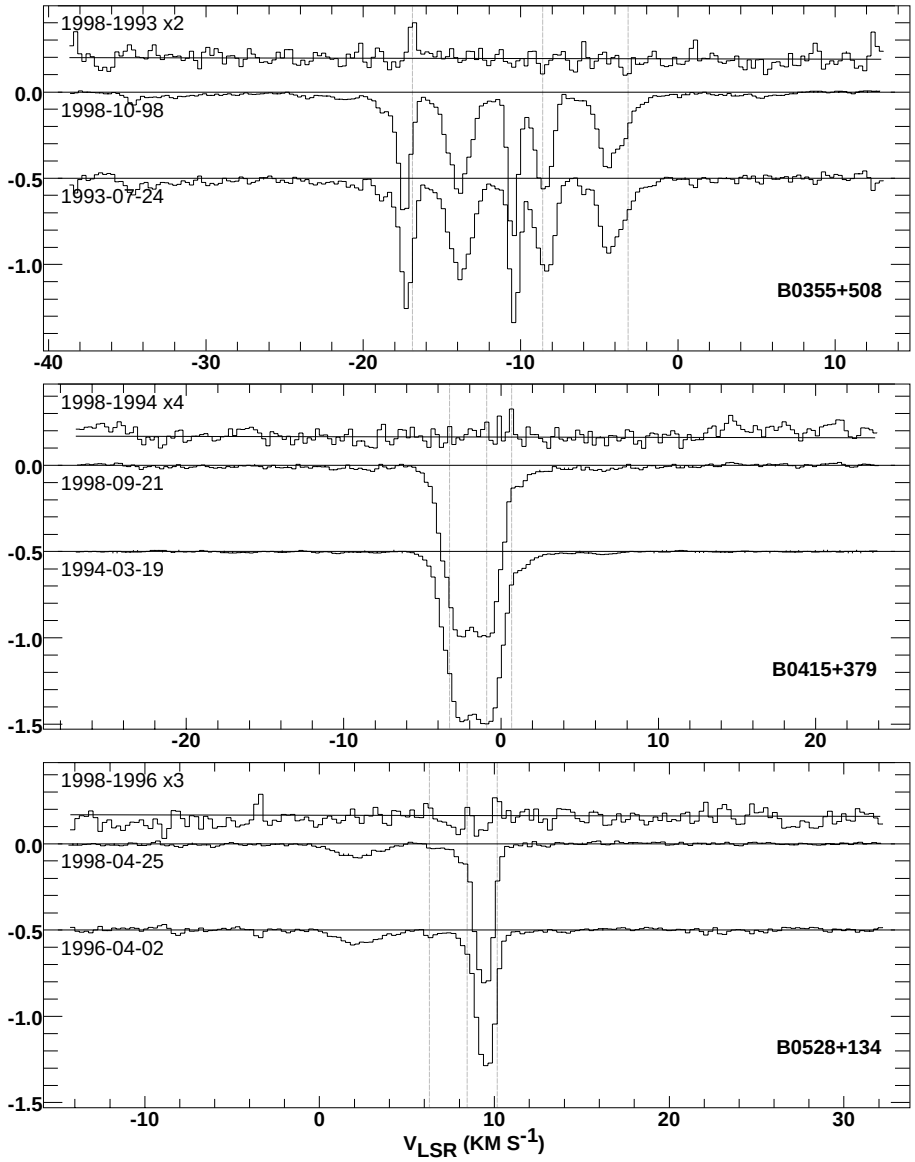

Fig. 1. HCO^+ spectra from two epochs and their difference, scaled as indicated

Table 2. OH Profile Integrals (km s^{-1})

Source	$< V >$ km s^{-1}	$\int (1-e^{-\tau})dv$ Old	$\int (1-e^{-\tau})dv$ New	$\int (1-e^{-\tau})dv$ BU
B0212+735	−10.9	−0.0139(0.0028)	−0.0100(0.0035)	
	−0.1	−0.0140(0.0018)	−0.0177(0.0019)	
	3.5	−0.1430(0.0024)	−0.1491(0.0026)	
B0355+508	−20.8	−0.0076(0.0025)	−0.0112(0.0022)	
	−17.4	−0.0367(0.0030)	−0.0419(0.0026)	−0.0345(0.0060)
	−13.9	−0.0268(0.0038)	−0.0206(0.0031)	−0.0285(0.0069)
	−10.4	−0.0453(0.0025)	−0.0350(0.0022)	−0.0424(0.0050)
	−8.5	−0.0345(0.0030)	−0.0287(0.0027)	−0.0332(0.0053)
	−4.1	−0.0342(0.0041)	−0.0278(0.0036)	−0.0400(0.0077)
	all	−0.1865(0.0088)	−0.1767(0.0078)	−0.1789(0.0140)
B0415+379	all	−0.4093(0.0190)	−0.4720(0.0127)	−0.4707(0.0240)
B1730−130	all	−0.0233(0.0018)	−0.0176(0.0018)	
B1954+513	all	−0.0474(0.0039)	−0.0417(0.0038)	
B2200+420	all	−0.0886(0.0041)	−0.0657(0.0028)	−0.0785(0.0058)

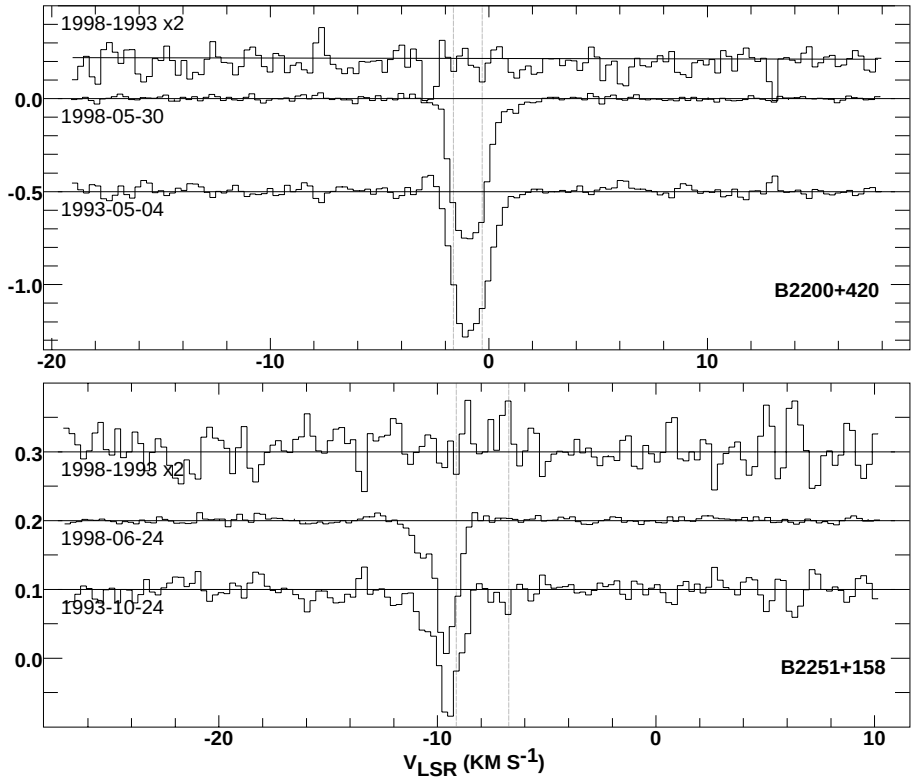

Fig. 2. HCO^+ spectra from two epochs and their difference, scaled as indicated

Table 3. HCO^+ Profile and Optical Depth Integrals (km s^{-1})

Source	Old	$< V >$	$\int (1-e^{-\tau})dv$ Old	$\int (1-e^{-\tau})dv$ New	$\int \tau dv$ Old	$\int \tau dv$ New
B0355+508	1993.6	−17.4	−0.892(0.023)	−0.856(0.006)	1.258(0.040)	1.172(0.009)
		−13.9	−1.048(0.022)	−1.034(0.005)	1.354(0.035)	1.337(0.009)
		−10.4	−0.736(0.017)	−0.767(0.004)	1.184(0.045)	1.258(0.012)
		−8.5	−0.811(0.021)	−0.832(0.005)	1.047(0.032)	1.089(0.009)
		−4.1	−0.904(0.030)	−0.981(0.008)	1.069(0.024)	1.160(0.009)
		all	−4.360(0.051)	−4.418(0.011)	5.888(0.190)	5.979(0.044)
B0415+379	1994.3	all	−3.990(0.005)	−4.060(0.013)		
B0528+134	1996.3	2.4	−0.241(0.013)	−0.226(0.009)	0.249(0.014)	0.233(0.010)
		9.4	−1.115(0.011)	−1.130(0.007)	1.781(0.022)	1.842(0.019
		all	−1.395(0.019)	−1.384(0.013)	2.030(0.028)	2.075(0.022)
B1730−130	1994.1	all	−0.850(0.046)	−0.911(0.014)	1.035(0.055)	1.134(0.027)
B1954+513	1994.3	all	−0.966(0.064)	−0.981(0.022)	1.395(0.100)	1.665(0.070)
B2200+420	1993.4	all	−1.446(0.030)	−1.496(0.012)	2.318(0.072)	2.368(0.033)
B2251+158	1993.8	all	−0.278(0.024)	−0.261(0.005)	0.299(0.024)	0.280(0.005)

HCO^+ profile integrals are presented in Table 3, where the column labelled 'Old' gives the epoch at which the older data were finalized. Differences between our old and new values are small and usually of little significance. The total profile integrals summed over all components are stable at the level of 1% in the best cases. For B0355+508 there is a pattern whereby the old integrals for individual components are greater toward the blue end and smaller to the red; this pattern is not repeated in OH, suggesting that it is due to some unrecognized systematic effect. The difference in profile integrals toward B0415+379 is significant in terms of the channel to channel rms error but is 1.7% overall. Evidence for variation in the OH toward this source is equivocal.

3.2. OH, then and now

OH profile integrals for $\int (1-e^{-\tau})dv$ are given in Table 2 along with results of (Moore and Marscher 1995) and (Marscher et al. 1993) (labelled 'BU') courtesy of A. Marscher who kindly forwarded his profiles. As noted in (Liszt and Lucas 1996), these BU data were actually used to normalize our old profile toward B0355+508; the profile inte-

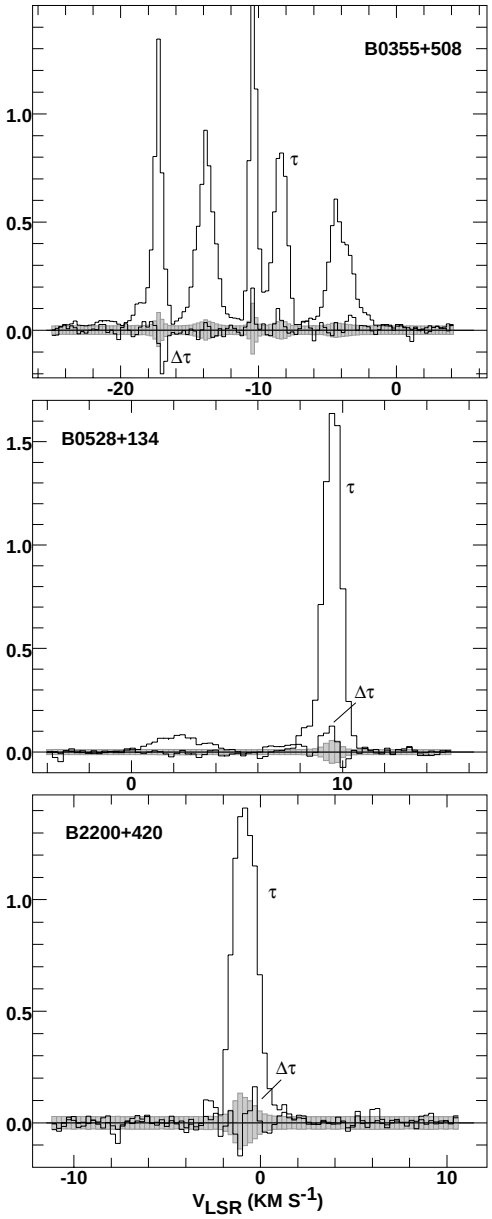

Fig. 3. Epoch 1998 optical depth spectra of HCO^+ toward three sources, and the difference optical depth spectrum from our new and old data. The shaded envelope is the optical depth difference for a $\pm 1\sigma$ change in the line-to-continuum ratio of the noisier of the two spectra used to form the difference

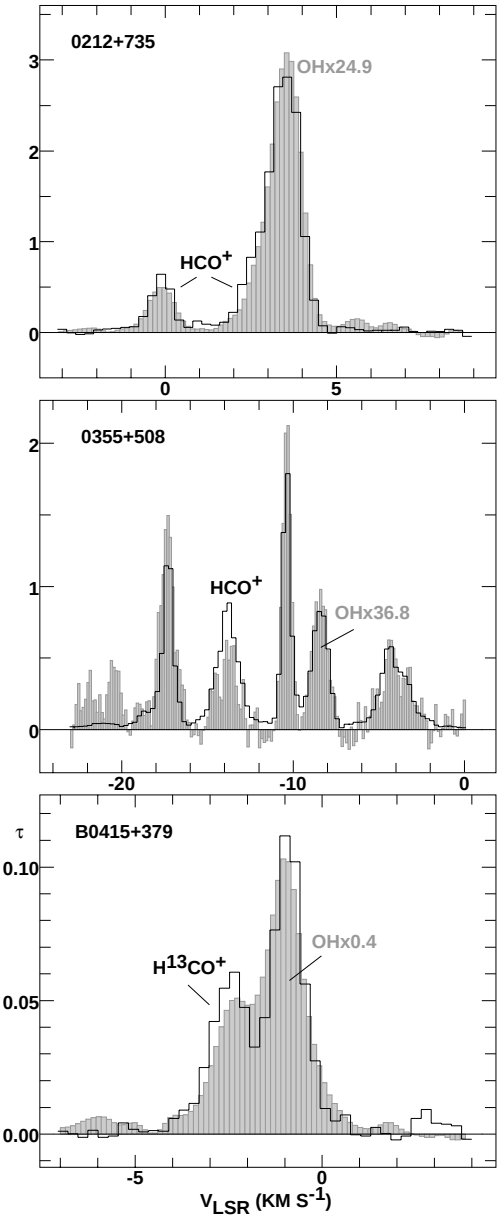

Fig. 4. HCO^+ and OH optical depth profiles. Data are from 1998 except for HCO^+ toward B0212+735 and $H^{13}CO^+$ toward B0415+379 which date from 1995 and have lower spectral resolution. The OH spectra have been scaled as indicated to have equal integrated optical depth

grals at v ≥ -20 km s^{-1} were set equal, so that only the distribution of absorption among the various components may be compared. The BU data agree very well with ours for the individual components, suggesting that some of the time-variability between our old and new data is real. In particular, the -10.4 km s^{-1} line changes by 3σ. But this component of the HCO^+ shows only a slight, opposite change.

The total profile integrals differ significantly between our old and new data in a few cases, most notably B2200+420 and B0415+379. Yet in each case, the BU data are closer to our newer results and the observed variations are not repeated in the HCO^+ profiles.

3.3. Comparison of HCO$^+$ and OH profiles

This comparison is illustrated in Figs. 4 and 5 where we have superposed the HCO^+ and OH optical depth profiles (without any adjustment of the velocity axes). The OH has been normalized to the same total area, except for B0212+735 and B1730−130 where only the area under the stronger line was set equal. The velocity resolution for the newer HCO^+ data is 0.23 km s^{-1} with 0.131 km s^{-1} channel separation but two of the HCO^+ profiles in the comparison are older and have lower resolution; for B0212+735 we have only the 0.47 km s^{-1} resolution data from our earlier epoch and toward B0415+379 the comparison

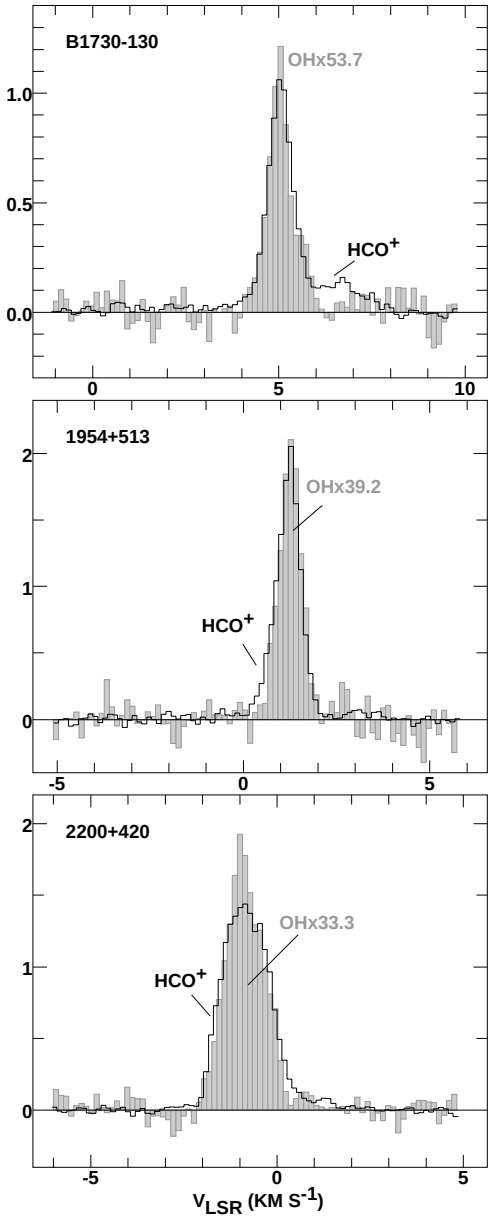

Fig. 5. 1998 HCO^+ and OH optical depth profiles. The OH spectra have been scaled as indicated to have equal integrated optical depth. Here and in Fig. 4, the OH has been convolved down to the resolution of the HCO^+

is made with $H^{13}CO^+$ (since the main HCO^+ line is so strongly saturated) for which the velocity resolution is 0.49 km s^{-1}. The OH spectra were convolved down to the appropriate resolution but kept at their original channel separation of 0.137 km s^{-1}.

In general, the profiles of these two species are very similar as befits their tight correlation of abundance. The extent of both species is sensibly identical but the -21 km s^{-1} line of OH toward B0355+508 is very weak in HCO^+ and the +7 km s^{-1} red wing of the HCO^+ line toward B1730$-$130 is absent in OH. There is a somewhat narrower line core in OH toward BL Lac and perhaps also in the stronger line toward B0212+735 (where the spectral resolution of the HCO^+ is low). The blue wing of the profile toward B0415+379 is relatively weak in OH when compared to either HCO^+ isotope, suggesting a partial kinematic decoupling of these (usually) chemically tightly-linked species. If there are other means of forming CO in a regime where H_3^+ chemistry is well-developed, there are routes to HCO^+ formation which do not involve OH. But the OH/HCO^+ ratios are entirely typical toward 3C111. In (Lucas and Liszt 1998) we noted that the carbon isotope ratios in the blue component are unusual in some species.

Single-component Gaussian fits to the lines do not show a clear pattern of differences in the line widths; for the strong lines toward B0212 and B1730, and for B1954, HCO^+ is 4%$-$8% broader (FWHM linewidths of 1.18, 0.77, and 0.77 km s^{-1} for HCO^+ *vs* 1.13, 0.71 and 0.72 km s^{-1}). Toward B0355, HCO^+ in the three stronger lines is narrower (0.61, 0.51, and 1.07 km s^{-1} *vs* 1.02, 0.58, and 1.08 km s^{-1}). Toward B2200, a one component fit gives a much broader HCO^+ line, 1.47 km s^{-1} *vs* 1.24 km s^{-1} but the HCO^+ line is really compound, composed of two slightly-separated components of nearly equal strength which simply cannot be well-decomposed by Gaussian fitting. The weaker line toward B0212+735 is narrower in HCO^+, 0.75 *vs* 0.94 km s^{-1}.

Sadly, we note briefly that the HCO^+ and OH lines are too narrow and too similar to be explained by profiles such as those shown for C-shock models by (Flower and Pineau Des Forêts 1998), which otherwise do a good job in reproducing the correlation of abundances. The double nature of the OH profiles in these models, arising from contributions from both the host (quiescent) and shocked gas, is not seen. In most cases, it is the HCO^+ which has the wider lines in absorption. However, it should be noted that the optical depth of OH is very sensitive to its excitation and this is not understood at the moment (Liszt and Lucas 1996): OH excitation temperatures should generally be much higher than they are (typically, only 1 K above the 2.7 K background) with a consequent reduction in the line optical depths.

4. A broad, underlying Galactic component of molecular absorption

The HCO^+ profiles in Figs. 1 and 2 toward B0355+508, B0415+379, and B1730$-$130 have a weak, broad underlying component which we have chosen not to ascribe to the individual clouds which provide the few strong features. Figs. 6 and 7 show why this is so. In each case, but most spectacularly the low-latitude object B0355+508, the HCO^+ is contiguous with the velocity ranges where HI absorption is prominent. The broad wings seem galactic in origin, from gas which is widely dispersed.

4.1. Equilibrium models of the gas

To understand the presence of this interesting new component of interstellar absorption profiles, we constructed a model of the H-H_2 and C^+-CO transitions in diffuse/translucent gas of

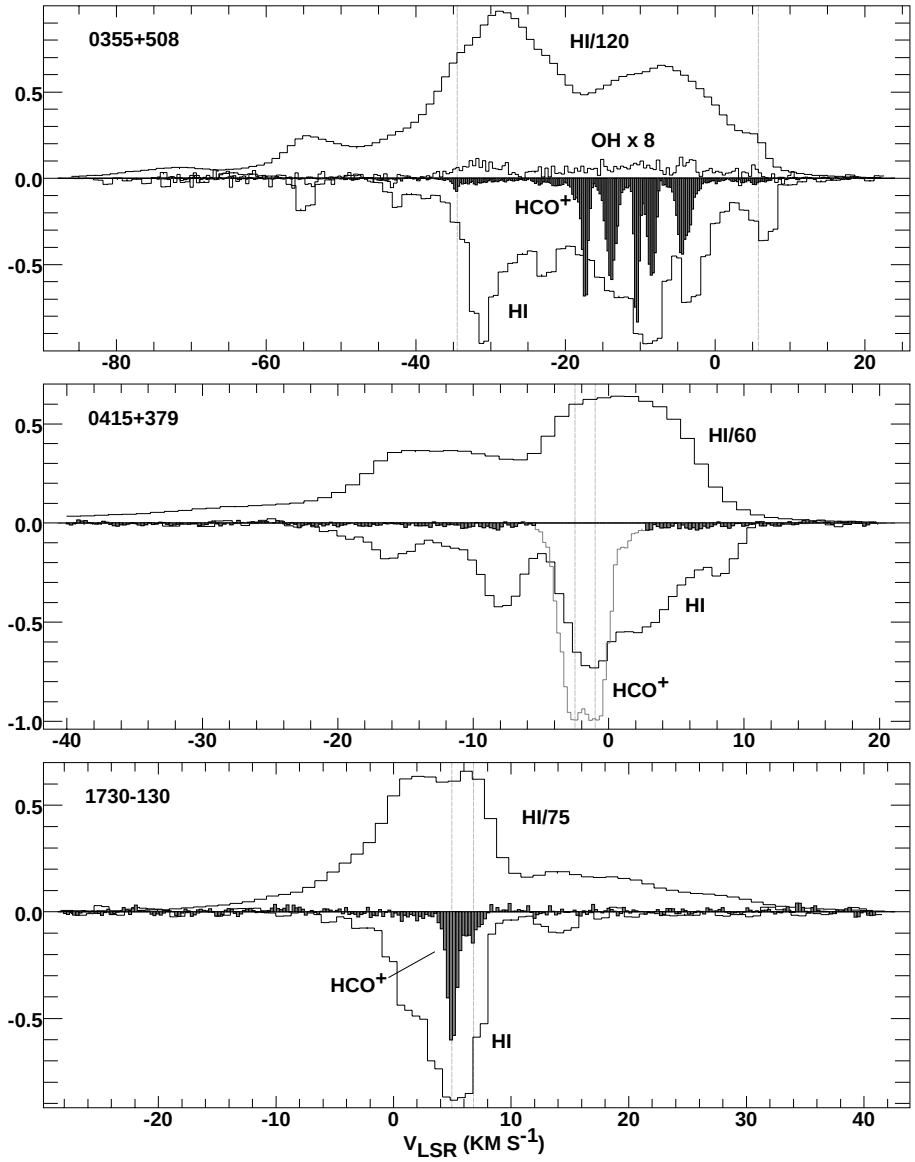

Fig. 6. Comparison of HCO^+ absorption with HI absorption and emission. HI absorption spectra are from (Dickey et al. 1983; Garwood and Dickey 1989). Emission data are the nearest profile from the all-sky survey of (Hartmann and Burton 1997). The absorption spectra are in the form of line/continuum − 1, the (scaled) emission spectra have units of Kelvins

small-to-moderate density, since these are the conditions under which the lines appear to form.

The calculations were initially begun as models of dense inclusions in diffuse clouds, such as might be called upon to explain the observed fluctuations in our HCO^+ profiles; the consequences of these models for just such a circumstance are explored later, in Sect. 5. We divided a model gas sphere of constant total density of H-nuclei into 64 radial zones and iteratively determined the H and H_2 abundances using the dust and self-shielding factors and the free-space photodissociation rate of (Lee et al. 1996), and a cosmic-ray ionization rate $\zeta_{\rm H} = 3 \times 10^{-17}$ s^{-1}. The anisotropy of the model's internal photon field is taken into account by a numerical integration over solid angle for each zone, and the model was assumed to be illuminated isotropically at its periphery. The interstellar radiation field scales with G0, G0 = 1 being the standard value. We took G0 = 0.65 for the calculations here because that leads to a thermal pressure (density-temperature product) near 3000 cm^{-3} K in purely atomic gas, with our chosen carbon depletion of a factor 2.5 with respect to the Solar value (see the annotations on the larger plot in Fig. 11).

Because the rate constant for the formation of H_2 on grains varies as $R_{\rm H_2} = 3 \times 10^{-18} \sqrt{T_{\rm kin}}$ cm^3 s^{-1} (Spitzer 1978), even a calculation of the H-H_2 transition makes it necessary to do the ionization, heating, cooling, and chemical calculations which simultaneously and self-consistently determine $T_{\rm kin}$ and the relative abundances of CI, C^+, CO, HI, H_2 and electrons. For the heating, we included terms corresponding to: cosmic ray ionization of hydrogen, releasing 6.6 eV of heat per event; photoionization of CI, releasing 1.16 eV; heating due to photoelectrons ejected from grains (Bakes and Tielens 1994); and heating due to the formation of H_2 on grains, releasing 3.4 eV per event. The cooling included: H-H_2 interactions (Martin et al. 1996); excitation of the fine-structure lines of CI, OI, and C^+ by electrons and H-atoms (Hollenbach and McKee 1989) and H_2 (Monteiro and Flower 1987; Schroeder et al. 1991;

Jaquet et al. 1992); and cooling due to CO including levels up to J=9. Of the cooling transitions, even the CO lines are not thick enough in diffuse clouds to require much attention to the radiative transfer. After some experimentation with more sophisticated methods, we finally did this rather crudely, calculating the local source function using an LVG code and forming the emergent line brightness by integrating the source function along the line of sight. The shielding factors needed to calculate the local abundance of CO were also taken from the work of (Lee et al. 1996).

The results shown here are for the mean (area-weighted) line of sight through the model cloud, intersecting it at an impact parameter equal to two-thirds of the radius. In comparing these models with the direct results of a simple LVG calculation for a bit of gas at constant density and temperature, we find that the non-uniform construct is substantially better at providing for the observed line ratios well up the rotation ladder.

The observed abundance of CO in gas threaded by a largely unattenuated interstellar radiation field cannot be reproduced by standard models of interstellar chemistry at low-to-moderate extinction and density: because they fail by one or two orders of magnitude to reproduce the observed abundances of polyatomics like HCO^+ which are the chemical antecedents of CO, standard models underproduce CO in like degree (Liszt and Lucas 1994). Current attempts to explain the observed high molecular abundances in thin gas columns invoke shocks which do not seem to reproduce the profiles we observe (Sect. 3.3) or take the form of somewhat esoteric-seeming discussions of energy dissipation in turbulent microstructures (Joulain et al. 1998) which we could not figure out how to adapt to this work. Here, the microscopic chemistry of CO formation is represented by a $single$ reaction $HCO^+ + e \rightarrow CO + H$ proceeding with a rate constant $3 \times 10^{-5}/T_{\rm kin}$ $\rm cm^3\ s^{-1}$ (as in the UMIST database), and with the relative abundance $n(HCO^+)/n(H_2)$ $assumed$ fixed at the observed value of 2×10^{-9} (Liszt and Lucas 1996). This simple $ansatz$ produces CO in the proper amount to explain the observations of CO emission, absorption, excitation, and isotopic fractionation discussed by (Liszt and Lucas 1998).

4.2. Weak Galactic HCO^+ absorption and the H-H_2 transition in diffuse clouds

As Fig. 8 shows, molecular hydrogen can achieve high abundance in clouds of rather low number density if $N(H) \geq 3 \times 10^{20}$ $\rm cm^{-2}$, $i.e.$, when the column density is above that of the 'standard' atomic hydrogen cloud (Spitzer 1978). Although the existence of an abrupt H-H_2 transition is due to dust and self-shielding, the high H_2 abundance comes about in part because the temperature is higher in more diffuse gas, the formation rate increases as $\sqrt{T_{\rm kin}}$, and H_2 formation can be an important source of heating. Of course this cannot continue indefinitely since (for example) the residence time of H-atoms on grains declines at higher temperature (as pointed out to us by the referee, Dr. John Black), but it is quite important within the context of the present models, over the range of temperatures inferred for clouds observed in λ21cm hydrogen absorption. The molecular hydrogen fractions shown here are noticeably higher than would have been the case had we approximated the H_2 formation rate by its value at, say, 60 K.

If HCO^+ forms along with H_2 itself, its weak underlying absorption would be a new diagnostic for the presence of H_2 in the ISM. So we would like to know how large a fraction of molecular gas and what HCO^+ abundance are required in order to explain the HCO^+ we see. To do this, we compare properties derived from the profile integrals of HCO^+ and HI. Toward B0355+508, for instance, the HI absorption may be said to occur in four ranges; $-57 \leq v \leq -37$ $\rm km\,s^{-1}$ where there is no accompanying HCO^+; $-37 \leq v \leq -20$ $\rm km\,s^{-1}$ and $0 \leq v \leq 10$ $\rm km\,s^{-1}$ where HCO^+ is weak; and $-20 \leq v \leq 0$ $\rm km\,s^{-1}$ where HCO^+ is strong. In Table 4 we show properties of the HCO^+ and HI spectra integrated over these ranges. The HCO^+ optical depth integral is converted into an equivalent column of H-nuclei assuming $HCO^+/H_2 = 2 \times 10^{-9}$ and $N(HCO^+) = 1.03 \times 10^{12}$ $\rm cm^{-2}$ $\int \tau dv$, applicable in the limit of no collisional excitation. The HI optical depth integral is converted into a column density N(HI) by calculating a spin temperature at each velocity, $T_{\rm sp}(v) = T_{\rm B}(v)/(1 - {\rm e}^{-\tau(v)})$ and integrating $T_{\rm sp}\tau$ over the line profile. For the more opaque regions of the spectrum, this HI column density is 70−80% higher than the optically thin limit $N(HI) = 1.823 \times 10^{18}$ $\rm cm^{-2}$ $\int T_{\rm B} dv$. The table gives the mean $T_{\rm sp}$ (weighted by optical depth) and shows results for various velocity ranges toward B0415+379 and B1730−130. The last column is the molecular fraction of the gas, given the assumptions.

Estimates for the molecular fraction in the ISM locally are 25% − 50%. The usually-quoted value for the local density of neutral gas at z = 0 is 1.2 $\rm cm^{-3}$ from surveys of extinction (Spitzer 1978) and no consistent interpretation of the 21 cm line will allow a local average of more than 0.6−0.7 $\rm cm^{-3}$ (Liszt 1983; Dickey and Lockman 1990). In any case, it follows from the table entries that the molecular fractions needed to reproduce the weak broad HCO^+ are at or below the local average. Of course the gas in question is not all local and the molecular gas fraction is declining at the Solar Circle but it seems that our observations really demand only one new thing of the interstellar medium: that the relative abundance of HCO^+ generally be of order 2×10^{-9} wherever the fractional abundance of H_2 is appreciable. Given this, the entire distributed molecular absorption component toward B0355+508 may be explained by gas associated with less than 0.25 magnitude of visual extinction.

Lack of detailed knowledge of the Galactic velocity field is a substantial barrier to calculating obvious quantities such as the mean density along the line of sight. A flat rotation curve viewed toward B0355+508 reaches -10 $\rm km\,s^{-1}$ at about 1 kpc distance, -20 $\rm km\,s^{-1}$ at 2.2 kpc, and -40 at 5.5 kpc (R = 13.5 kpc), for R_0 = 8.5 kpc. Roughly speaking, the mean density of molecular material associated with the strong HCO^+ absorption from 0 to -20 $\rm km\,s^{-1}$ is then just 0.90 (H-nuclei) $\rm cm^{-3}$, and that of the atomic gas perhaps 0.67 $\rm cm^{-3}$. For the negative-velocity region of weak HCO^+ absorption the mean densities

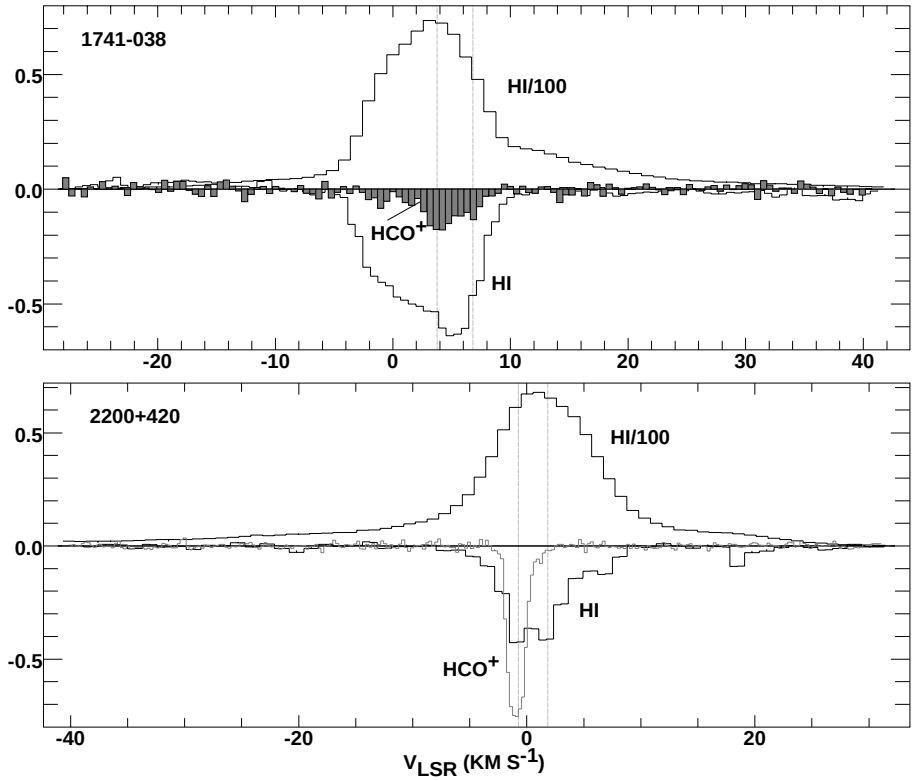

Fig. 7. Comparison of HCO^+ absorption with HI absorption and emission, as in Fig. 6

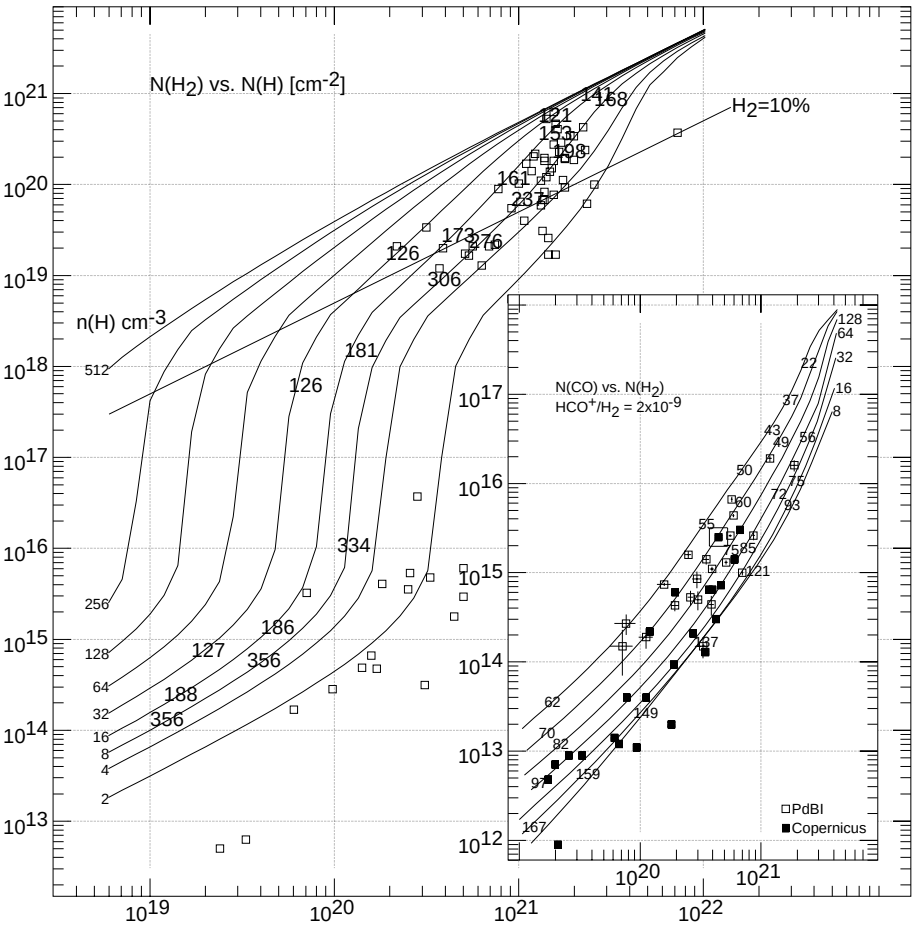

Fig. 8. Outer frame: Variation of computed H_2 column density with total hydrogen column density. The curves are for model gas spheres of various density, as indicated, with mean equilibrium kinetic temperatures noted. The $Copernicus$ data of (Savage et al. 1977) are shown as open squares. Inset: Calculated CO column density $vs.$ N(H_2) for number densities n(H) = 8, 16, 32...512 cm^{-3} as indicated. UV absorption measurements summarized in an updated version of the summary in (Federman et al. 1994), mostly from $Copernicus$, and our λ2.6mm absorption line data (Liszt and Lucas 1998) are shown as filled and open symbols, respectively. Both the models and the mm-wave data assume that $[\mathrm{HCO}^+]/[\mathrm{H}_2] = 2 \times 10^{-9}$. Mean kinetic temperatures weighted by N(CO) are shown. The data toward the star ζ Oph are shown outlined

Table 4. Molecular and atomic column densities toward three sources

Source	Range km s^{-1}	$\int \tau(\mathrm{HCO^+})dv$ km s^{-1}	2N(H_2) cm^{-2}	$\int \tau(HI)dv$ km s^{-1}	$\int T_\mathrm{B}dv$ K km s^{-1}	$<T_\mathrm{sp}>$ K	N(HI) cm^{-2}	f_{mol}
B0355+508	(−57,−37)	0	0	1.40	477	472	1.22E21	0
	(−37,−20)	0.40	0.41E21	14.97	1694	170	4.74E21	0.08
	(−20,0)	5.95	6.13E21	24.35	1383	103	4.56E21	0.57
	(0,10)	0.14	0.14E21	2.67	300	127	0.62E21	0.18
B0415+379	(−24,−5)	0.23	0.24E21	3.32	327	108	0.66E21	0.26
	(−5,7)	13.3	13.7E21	8.47	427	46	1.09E21	0.93
	(7,10)	0.03	0.04E21	0.66	51	86	0.10E21	0.26
B1730−130	(−8,4)	0.10	0.10E21	3.94	319	100	0.72E21	0.13
	(4,8)	1.06	1.09E21	7.29	276	71	0.94E21	0.54
	(8,33)	0.06	0.06E21	0.66	268	416	0.50E21	0.11

are 0.47 cm^{-3} and 0.04 cm^{-3} for the atomic and molecular components, respectively.

4.3. What forms the carbon monoxide we see in diffuse clouds?

There is an implication of ubiquitous HCO^+ which deserves to be noted. Inset in Fig. 8 is a plot of predicted and observed CO column densities as a function of N(H_2). The observed values of N(CO) from UV absorption measurements, summarized in an updated version of the summary in (Federman et al. 1994), are shown as filled symbols and are labelled $Copernicus$. The open symbols are our measurements from the Plateau de Bure (Liszt and Lucas 1998) of N(CO)/N(HCO^+), adjusted along the horizontal axis so that $N(\mathrm{HCO^+})/N(\mathrm{H_2}) = 2\times10^{-9}$, similar to what we derived in our prior discussion of OH and the OH-HCO^+ correlation (Liszt and Lucas 1996). The mm-wave data overlap with the UV absorption measurements at their high end, and extend the range of empirically-determined behaviour by about one order of magnitude in N(CO).

Shown are the predictions of our models at various number densities, with the self-consistently determined, CO abundance-weighted kinetic temperatures shown as numbers at some locations in the plane, again for a constant abundance ratio $N(\mathrm{HCO^+})/N(\mathrm{H_2}) = 2\times10^{-9}$. It is the case, that with only one assumption – this ubuiquitous, high abundance of HCO^+ relative to H_2 – the run of N(CO) $vs.$ N(H_2) can be explained over a factor of more than 10^4 in N(CO). A proportionality N(CO) $\propto$ N$(\mathrm{H_2})^2$ occurs naturally around N(CO) = $10^{15}\mathrm{cm}^{-2}$

We view this as a confirmation of the claim made earlier (Liszt and Lucas 1994), that the formation problem for CO in conventional models of the diffuse cloud chemistry is a problem of supply – a too-low formation rate – not any gross overestimation of the photodestruction rate. When HCO^+ is present at its observed abundance, it follows without further assumptions that the observed quantities of CO form by electron-HCO^+ recombination, even in the presence of a high CO photodestruction rate.

5. Dense inclusions in diffuse clouds?

5.1. Profile variations in HCO^+ absorption lines

Profile variations in molecular gas over time have been discussed by (Moore and Marscher 1995) and (Marscher et al. 1993); (Diamond et al. 1989) and (Faison et al. 1998) present VLBA maps of strong ($\Delta\tau \approx 1$) variations in HI optical depth. In both cases, it is suggested that AU-sized inclusions are needed to reproduce such high degrees of variability on yearly or milli-arcsecond scales. More or less the same considerations apply here, except that the column densities and column density differences are typically much greater in molecular gas compared to HI.

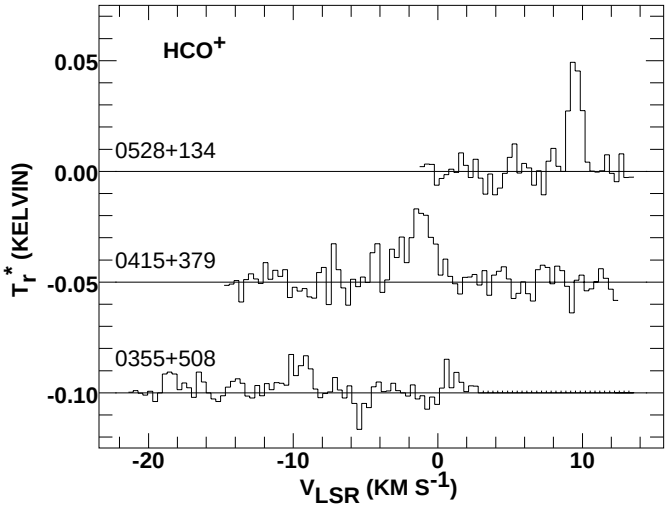

Fig. 9. HCO^+ emission spectra toward three sources, from (Lucas and Liszt 1996)

The existence of AU-sized structure in pc-sized clouds, producing 10% − 100% changes in optical depth, seems to imply the presence of some kind of inclusion having a local number density 0.1 − 1.0 x 206265 higher than in the ambient material. Since most profiles seem subject to variability (at least from the references cited), these extreme conditions are common. Since the profile variations occur as fluctuations, rather than disruptions, of a template profile, even this extreme material somehow partakes of normal cloud kinematics.

(Heiles 1997) recently discussed the (in retrospect) rather mild fluctuations which are seen in HI absorption spectra toward pulsars (Frail et al. 1994) where 2 km s^{-1}-wide changes with $\Delta\tau(HI) \approx 0.1$ commonly occur. This implies a column density variation of only $4\times10^{17}T_\mathrm{kin}\mathrm{cm}^{-2}$: by careful tuning, and by considering a very dense underlying atomic cloud

($100\ \mathrm{cm}^{-3}$), he was able to lower the required over-densities and pressures considerably. Heiles noted that if his model inclusions were to be very cold (needed to lower the column density associated with a given level of fluctuation in the optical depth) they would cool by CO emission with line brightnesses just at/above the nominal 0.3K sensitivity limits of surveys like those used to define our sample of background objects (Liszt and Wilson 1993; Liszt 1994). In suggesting a more sensitive search for these lines in emission, he neglected the fact that the CO in any such features would readily have been manifested in absorption, and in related molecules as well, and is not seen (*ibid*, (Liszt and Lucas 1996)).

Stellar extinction measurements conducted by Thoraval and her collaborators (Thoraval et al. 1996, 1997) put interesting constraints on the small-scale structure of extinguishing material of moderate column density. In time series, it is found that stars do not vary in brightness as dark masses temporarily occult them. In spatial extinction maps, the fluctuations are such that the column density is smoothly distributed, without extremes. This means that any internal cloud structure responsible for variation in spectral line profiles cannot contain a large fraction of the total amount of material through a typical line of sight.

Here we show that our measurements, although exhibiting the same profile variations, also bear strong direct evidence that the usual dense molecular concentrations within clouds are not the cause. These arguments could probably have been adduced earlier and are not terribly subtle. Shown in Fig. 9 are HCO^+ emission profiles from our earlier survey (Lucas and Liszt 1996), to make the point that HCO^+ emission is very weak toward our sources, typically below 0.05K. This is consonant with the low thermal pressures deduced from CO absorption (Liszt and Lucas 1998). In Fig. 10, we show the result of a very straightforward HCO^+ excitation calculation for a bit of gas bearing a column $N(\mathrm{HCO}^+) = 10^{12}\ \mathrm{cm}^{-2}$ over a 1 $\mathrm{km\,s}^{-1}$ velocity interval. The calculation is parametrized by the temperature and density; we have assumed that a piece of molecular gas is exposed to the interstellar radiation field and determined the electron density with carbon depleted in abundance by a factor of 2.5 from the Solar value; the standard free-space carbon photoionization rate $\Gamma_C = 2.2 \times 10^{-10} s^{-1}$; and a cosmic-ray ionization rate of $\zeta_H = 3 \times 10^{-17} s^{-1}$. Knowing n($H_2$), n(e), $T_{\rm kin}$, and N(HCO^+) we can calculate the line brightness and optical depth, which we have plotted.

At densities of $n(\mathrm{H}_2) = 100\ \mathrm{cm}^{-3}$, the observed line emission brightnesses and optical depths are produced naturally by the conditions which prevail in diffuse clouds, without extra assumptions. At such low density, all the curves for the optical depth coincide when the excitation is minimal: they separate substantially at higher density, depending on the temperature, as population is shifted into the upper levels. At high density, $\mathrm{n}(\mathrm{H}_2) > 10^4 - 10^5\ \mathrm{cm}^{-3}$, the predicted brightness temperature varies relatively little with either kinetic temperature or number density.

Consider the case that in a typical HCO^+ line with $\int \tau dv$ = 1.17 $\mathrm{km\,s}^{-1}$ (like that of the -17 $\mathrm{km\,s}^{-1}$ component toward B0355+508) equivalent to N(HCO^+) = $1.2 \times 10^{12}\ \mathrm{cm}^{-2}$ over a 1 $\mathrm{km\,s}^{-1}$ linewidth, we would try to induce an optical depth change like that which is shown in Fig. 3, with $\int \Delta\tau dv = 0.12$ $\mathrm{km\,s}^{-1}$. For gas at $T_{\rm kin}$= 30 K, n(H_2) = $10^5\ \mathrm{cm}^{-3}$, we infer from Fig. 10 that the column density of HCO^+ required would be $N(\mathrm{HCO}^+) = 1.2 \times 10^{12}\ \mathrm{cm}^{-2}$, which would produce HCO^+ emission of 1.4 K. Since that is more than 100 times higher than what is seen, less than 1% of the HCO^+ can exist at such conditions.

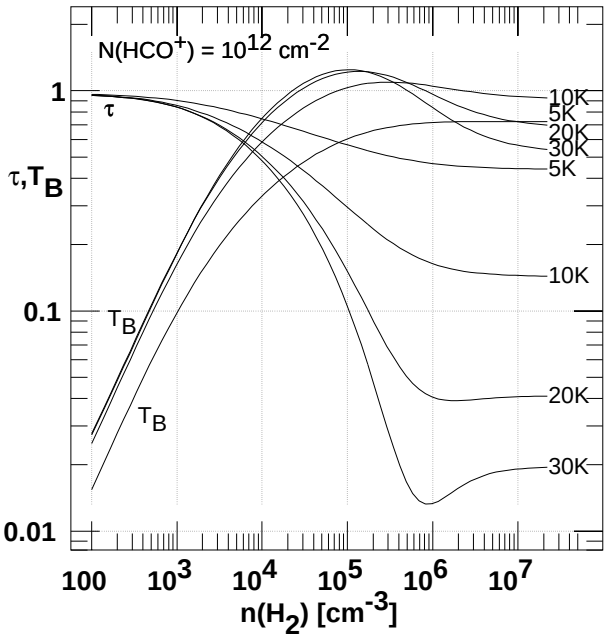

Fig. 10. HCO^+ J=1−0 optical depth and brightness temperature for a column $N(\mathrm{HCO}^+) = 10^{12}\ \mathrm{cm}^{-2}$ and linewidth $\sqrt{2\pi}\sigma_v = 1 \mathrm{km\,s}^{-1}$ at various densities and kinetic temperatures

Of course the density and temperature do not vary independently but this naive approach makes it clear that any dense inclusions would have to be composed of gas which is very cold, even though it is not strongly shielded. To see how cold such dense gas might be in equilibrium, we went through the exercise of calculating the temperature in a gas of moderate column density at various number densities. The results are as shown in Fig. 11 at top; the gas cannot be made arbitrarily cold as long as it is exposed to the interstellar radiation field. (Heiles 1997) calculated that (atomic) gas would not get colder than 13.5 K and we find 10−12 K as well. This is still warm enough to produce quite strong HCO^+ emission at high density, so that material at densities above (say) $10^4\ \mathrm{cm}^{-3}$ cannot include more than a few percent of the HCO^+ in any cloud.

As the gas becomes denser, it invariably makes the C^+-C-CO transition as well (Fig. 11 at bottom) and what begins as an attempt to induce relatively mild fluctuations in the HCO^+ optical depth produces unacceptably large amounts of CO. The abundance of CO increases by about a factor of 100 at high density, even at low extinction; thus, again, only about 1% of the gas can exist under such conditions.

5.2. HCO^+ profile variations are not caused just by extremely dense inclusions

The existence of a limit on the fraction of HCO^+ which can exist under extreme conditions is sufficient to eliminate the usual models of dense clumps, at least in the context of the present discussion of equilibrium conditions.

We want these inclusions to be commonly observable, seen of order half the time; this implies that the total amount of surface area in clumps is comparable to that of the cloud in which they are embedded. So let the ratio of total clump to cloud area be denoted by f_π: since the probability of encountering a clump along a random line of sight is $1-\exp(-f_\pi)$, $f_\pi \approx 0.7$ to give an even chance of encountering one clump per cloud. Next, denote the ratio of the HCO^+ column density in a clump to that through the cloud by f_{cl}: for the dense 30 K gas considered as an example in Sect. 5.1, f_{cl} was unity and would have been about 0.4 for gas at the same density but 10 K.

Then, the constraint from the emission, that only a fraction f_{em} of the HCO^+ can be at extreme conditions, may be expressed as $f_\pi \times f_{cl} \leq f_{em}$ and this is a problem. If f_π is fixed at a relatively high value of order unity to make the clumps commonly detected, and if f_{cl} is of order unity, there is no way to make their product be as small as it must be. Much smaller fluctuations or much less frequent variations can be explained, but only because they approach the limit of no variations.

These arguments are hardly unique to HCO^+ but apply to older observations of OH and as well.

5.3. Chemical and other fluctuations as the cause of profile variations in molecular absorption line profiles

The usual assertion (Moore and Marscher 1995) that molecular absorption line profile variations require small substructures of correspondingly high hydrogen volume density is really based on the implicit constancy of the molecular abundance, or, for that matter, all the other quantities affecting the optical depth: for OH in material of modest density, these are manifested in its poorly−understood excitation temperature. If the molecular abundance is allowed to vary widely, other, contradictory aspects of the problem largely disappear (for instance, the extinction need not vary). Especially in diffuse gas, where the chemistry is hardly driven to saturation, it would seem quite possible that large fluctuations in chemical abundance could easily be driven by local changes in ambient physical circumstances, for instance, due to the temporary dissipation of turbulent energy, the onset of bistability, and so forth.

As an example, consider the case where a fluctuation of size l (typically AU) in a cloud of size L (typically pc; L >> l) is required to harbor a column N_X of some species X whose relative abundance varies as $n_X/n_H \propto {n_H}^p$. It follows that the density over the l-sized region must be $n_H(l) \propto (L/l)^{1/(p+1)}$. In the usual case, p = 0 and $n_H \propto L/l$. But if p = 1, the required density increase is only $n_H \propto \sqrt{L/l}$, which is smaller by a factor > 100, and the column of hydrogen required over the l-sized fluctuation is reduced by the same factor. Clearly this sort of (chemical) inhomogeneity can go a long way toward alleviating difficulties in explaining the rapid variability of some molecular line profiles.

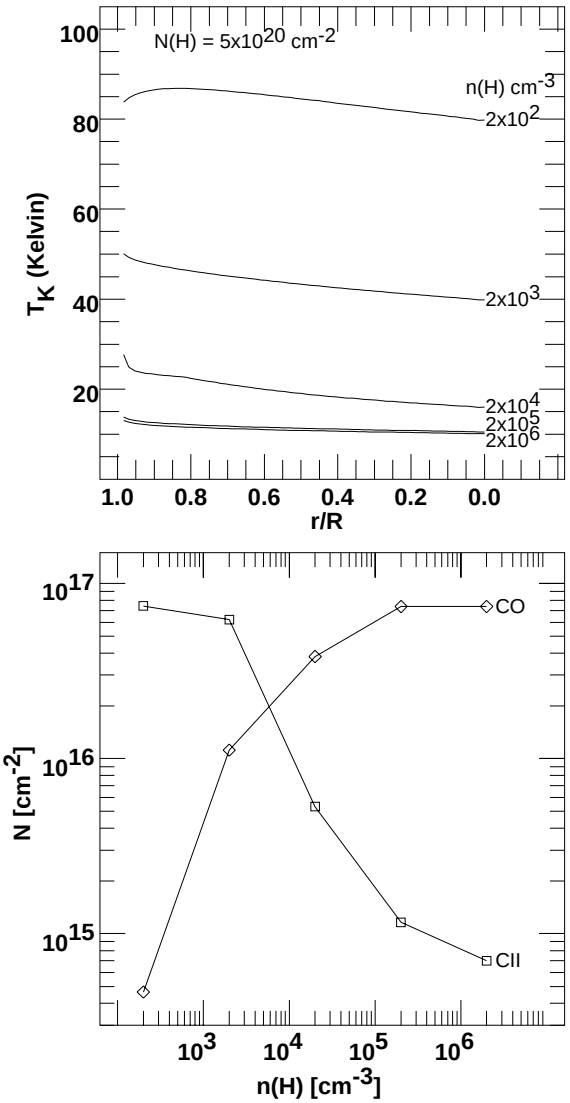

Fig. 11. Top: Variation of computed kinetic temperature across model gas spheres of various densities, for N(H) = 5×10^{20} cm^{-2}. Bottom: CO and C^+ column densities for the model gas spheres shown at top

The previous discussion relies on the assumption that a significant change in the molecular column density occurring while the line of sight is displaced by a small distance l across a cloud must originate in a relatedly small part $\sim l$ along that line of sight. This assumption might conceivably fail for some models of cloud structure: for instance in a cloud with density enhancements occuring in two-dimensional sheets, the main fluctuations in the column density as a function of impact parameter would occur when the line of sight tangentially hits one of these sheets, in which case the need for high density could be relaxed by a large amount, somewhat reminiscent of the geometrical tuning described by (Heiles 1997). Fractal models of diffuse clouds would actually be needed to investigate this point in detail.

6. Summary

We began by comparing OH and HCO^+ profiles taken over an approximately five year interval. Profiles are generally stable, but may exhibit small differences. Fig. 3 summarizes the results over time, showing profiles of the HCO^+ optical depth and optical depth difference, along with the spectrum of the expected variance. Variations of the sort observed in the strong lines toward B0528+134 and B2200+420 are largely integral-conserving and placed near the line center, and could in principle be explained solely as a slight velocity shift. Some of the variations seen toward B0355+508 are different in character – non-conserving, narrow and off-center. In general, the differences seen in HCO^+ are not obviously mimicked in OH (and *vice versa*). Overall, things seem to change at the level of 1%−2% only. Longer time baselines are required.

Between species, OH and HCO^+ profiles viewed at $0.14-0.24$ km s^{-1} resolution are disarmingly similar. There is no signature in the kinematics of macroscopic shocks – broad wings off narrow cores, profile doubling, $etc.$ – or of gross chemical differentiation. OH and HCO^+ lines have pretty much the same linewidths in the same components, while showing occasional small differences such as toward B1730−130 where the red wing of the HCO^+ line is missing in OH. Unfortunately the OH absorption profile does not bear the same direct optical depth - column density relationship applicable to HCO^+, because the OH excitation temperature is not negligible. So profile differences could in principle be explained by cloud substructure independent of the kinematics. The general absence of OH-HCO^+ optical depth profile differences should be useful in constraining internal cloud structure.

We found a new component of molecular absorption due to distributed gas, seen over the same range where the optical depth is appreciable in H I. Toward B0355+508 at b = -1.6^o the HCO^+ absorption extends continuously over more then 40 km s^{-1}, sampling gas out to R = 1.6 R_0. This behaviour can be straightforwardly explained by current estimates of the molecular gas fraction at/beyond the Solar Circle, if the abundance of HCO^+ has its typically observed value $HCO^+/H_2 = 2 \times 10^{-9}$ wherever H_2 forms in noticeable quantities. Using a model of the H-H_2 and C^+-CO conversion based entirely on physical mechanisms detailed in the literature, we showed that modern values of the various physical parameters predict that H_2 formation can occur at quite low densities, which accounts for the existence of gas which readily absorbs in the HCO^+ lines but emits little in mm-wave species (this gas does however appear in OH emission, at least toward B0355+508). We then pursued the consequences of this ubiquitous HCO^+ gas and showed through modelling that the observed behaviour of N(CO) $vs.$ N(H_2) can be explained solely by allowing HCO^+ to recombine to CO in otherwise standard diffuse cloud models.

Finally, we considered the nature of the cloud substructure which might be responsible for the ubiquitous profile variations seen in so many high-resolution line absorption experiments, including those exemplified in Fig. 3. For the diffuse but partially molecular gas, the weakness of HCO^+ emission is a powerful constraint: using it we were able to show very straightforwardly that it is impossible to construct a successful model of the usual kind in which small, dense clumps are supposed to produce frequent optical depth fluctuations while remaining unobtrusive in emission. Instead, we conclude that it is necessary to incorporate small-scale chemical and/or other inhomogeneities – a fractal geometry? – and that these will give the added latitude necessary to reproduce the rapidly-growing body of emission and absorption measurements of molecules in the diffuse interstellar medium.

Acknowledgements. The National Radio Astronomy Observatory is operated by AUI, Inc. under a cooperative agreement with the US National Science Foundation. We owe the staff of the VLA and at the Plateau de Bure our thanks for helping to take the data. The AIPS task UVLSD used to reduce our VLA OH data was written by Eric Greisen.

The comments of Dr. John Black, the referee, were gratefully received.

We dedicate this paper to the memory of six IRAM employees, Bernard Aubeuf, Francis Gillet, Henri Gontard, David Lazaro, Roland Prayer, Patrick Vibert, who lost their lives in 1999, in two terrible accidents.

References

Bakes, E. L. O. and Tielens, A. G. G. M.: 1994, ApJ 427, 822
Cox, P., Guesten, R., and Henkel, C.: 1988, A&A 206, 108
Diamond, P. J., Goss, W. M., Romney, J. D., Booth, R. S., Kalberla, P. M. W., and Mebold, U.: 1989, ApJ 347, 302
Dickey, J. M., Kulkarni, S. R., Heiles, C. E., and Van Gorkom, J. H.: 1983, ApJS 53, 591
Dickey, J. M. and Lockman, F. J.: 1990, Ann. Rev. Astr. Ap. 28, 215
Faison, M. D., Goss, W. M., Diamond, P. J., and Taylor, G. B.: 1998, AJ 116, 2916
Federman, S. R., Strom, C. J., Lambert, D. L., Cardelli, J. A., Smith, V. V., and Joseph, C. L.: 1994, ApJ 424, 772
Flower, D. R. and Pineau Des Forêts, G.: 1998, MNRAS 297, 1182
Frail, D. A., Weisberg, J. M., Cordes, J. M., and Mathers, C.: 1994, ApJ 436, 144
Garwood, R. W. and Dickey, J. M.: 1989, ApJ 338, 841
Hartmann, D. and Burton, W. B.: 1997, *Atlas of galactic neutral hydrogen*, Cambridge; New York: Cambridge University Press
Heiles, C.: 1997, ApJ 481, 193
Hollenbach, D. and McKee, C. F.: 1989, ApJ 342, 306
Jaquet, R., Staemmler, V., Smith, M. D., and Flower, D. R.: 1992, Journal of Physics B Atomic Molecular Physics 25, 285
Joulain, K., Falgarone, E., Des Forets, G. P., and Flower, D.: 1998, A&A 340, 241
Lee, H. H., Herbst, E., Pineau Des Forets, G., Roueff, E., and Le Bourlot, J.: 1996, A&A 311, 690
Liszt, H. S.: 1983, ApJ 275, 163
Liszt, H. S.: 1994, ApJ 429, 638
Liszt, H. S. and Lucas, R.: 1994, ApJ 431, L131
Liszt, H. S. and Lucas, R.: 1996, A&A 314, 917
Liszt, H. S. and Lucas, R.: 1998, A&A 339, 561
Liszt, H. S. and Wilson, R. W.: 1993, ApJ 403, 663
Lucas, R. and Liszt, H.: 1998, A&A 337, 246
Lucas, R. and Liszt, H. S.: 1993, A&A 276, L33, (LL93)
Lucas, R. and Liszt, H. S.: 1994, A&A 282, L5, (LL94)

Lucas, R. and Liszt, H. S.: 1996, A&A 307, 237, (LL96)
Marscher, A. P., Bania, T. M., and Wang, Z.: 1991, ApJ 371, L77
Marscher, A. P., Moore, E. M., and Bania, T. M.: 1993, ApJ 419, L101
Martin, P. G., Schwarz, D. H., and Mandy, M. E.: 1996, ApJ 461, 265+
Monteiro, T. S. and Flower, D. R.: 1987, MNRAS 228, 101
Moore, E. M. and Marscher, A. P.: 1995, ApJ 452, 671
Savage, B. D., Drake, J. F., Budich, W., and Bohlin, R. C.: 1977, ApJ 216, 291
Schroeder, K., Staemmler, V., Smith, M. D., Flower, D. R., and Jaquet, R.: 1991, Journal of Physics B Atomic Molecular Physics 24, 2487
Spitzer, L.: 1978, *Physical processes in the interstellar medium*, New York Wiley-Interscience, 1978. 333 p.
Thoraval, S., Boisse, P., and Duvert, G.: 1997, A&A 319, 948
Thoraval, S., Boisse, P., and Stark, R.: 1996, A&A 312, 973
Van Dishoeck, E. F. and Black, J. H.: 1988, ApJ 334, 771
Viala, Y. P., Roueff, E., and Abgrall, H.: 1988, A&A 190, 215